DOI: 10.61782/fa.2023.1201

forum acusticum 2023

A RE-CONFIGURABLE SUBWAVELENGTH SOUND ABSORBER BASED ON ACTIVE MEMBRANE-TYPE ACOUSTIC METAMATERIALS

Felix Langfeldt*

Institute of Sound and Vibration Research, University of Southampton,
University Road, Southampton, SO17 1BJ, United Kingdom

ABSTRACT

Membrane-type acoustic metamaterials (MAM) are composed of a thin, prestressed membrane with periodically attached masses. This design allows for a very thin and lightweight construction that, in combination with a back cavity, can achieve perfect sound absorption at subwavelength length scales. However, MAM-based sound absorbers achieve significant sound absorption values only in a narrow frequency band. This means that when tonal noise from sources with varying tonal frequencies (e.g. propeller engines) should be reduced using these absorbers, the noise reduction will be significantly impaired as soon as the tonal frequency of the source falls outside the sound absorption frequency band of the MAM. In this contribution, a preliminary investigation of an active MAM-based absorber with re-configurable sound absorption frequency bands will be presented. The proposed active MAM consists of a MAM with attached electrodynamic actuators and sensors, which could enable an in-situ modification of the MAM properties. An analytical model of the active MAM absorber will be used to study different sensor-actuator combinations that could be used to achieve the control of the sound absorption band over a wide frequency range.

Keywords: *acoustic metamaterials, active, sound absorption*

**Corresponding author*: F.Langfeldt@soton.ac.uk.

1. INTRODUCTION

Membrane-type acoustic metamaterials (MAM) have first been proposed in 2008 by Yang et al. [1] as a thin and lightweight acoustic metamaterial exhibiting frequency bands with negative effective density. MAM are made of a periodic arrangement of subwavelength sized unit cells, each consisting of a thin, prestressed membrane with one or more rigid masses attached to it. This arrangement forms a mass-spring system, which can, for example, exhibit frequency bands with negative effective density [1] and acoustic anti-resonances with sound transmission loss values that greatly exceed the transmission loss of a homogeneous plate with equivalent weight [2].

MAM can also be used to realize subwavelength perfect sound absorbers by mounting them in front of a thin, rigidly terminated fluid gap [3]. By properly tuning the properties of the MAM in relation to the fluid gap thickness, narrow frequency bands with sound absorption coefficients of up to 100 % with an absorber thickness of less than 1 % of the wavelength can be achieved [3]. While these properties of MAM absorbers are clearly advantageous for absorbing low-frequency tonal noise, the narrow bandwidth strongly limits their application to practical noise control problems. Mei et al. [4] could show that the bandwidth of MAM absorber panels can be improved by stacking multiple MAM layers on top of each other, but this counteracts one of the most appealing properties of MAM absorbers: their subwavelength thickness. For some applications (for example involving tonal noise from a propeller that rotates at different speeds) it might be sufficient to be able to adapt the frequency at which the MAM exhibits perfect absorption and track a tonal frequency in the incidence noise over a wide frequency range. For example, Xing et al. [5] exploited a static pres-

surization and the resulting geometrically non-linear stiffening (as first proposed in Ref. [6] for tuning the sound transmission loss of MAM) to re-configure the sound absorption peak of a MAM between 150 and 360 Hz using differential pressures of up to 12.8 kPa. This approach, however, requires a bulky air pump to generate the pressurization and leaks can make it difficult to sustain this pressure in practice.

In Ref. [7] it was shown that an active MAM with controllable anti-resonances can be realized for sound transmission problems by adding an electrodynamic actuator to the MAM and controlling it using a microphone measuring the pressure on the incident side of the MAM. The advantage of this design is that the actuators, sensors, and controllers can be integrated in a compact way on the added mass and no bulky additional systems would be required. Based on this, the aim of the present contribution is to investigate if and how this active MAM design can also be used to realize re-configurable subwavelength sound absorbers.

The paper is structured as follows: In Section 2, the analytical model which was used to predict the sound absorption coefficient α of the active MAM is described. In Section 3, this analytical model is first validated using experimental data from impedance tube measurements. Then, the model is applied to investigate the performance and stability of three different active MAM configurations. Finally, Section 4 will provide a brief summary and the conclusions of the main findings in this contribution.

2. ANALYTICAL MODEL

2.1 Sound Absorption Coefficient

The normal incidence sound absorption coefficient α of an absorber can be calculated using the matching law [8]:

$$\alpha = \frac{4\,\mathrm{Re}\{\mathcal{Z}\}}{(\mathrm{Re}\{\mathcal{Z}\}+1)^2 + \mathrm{Im}\{\mathcal{Z}\}^2}, \tag{1}$$

where $\mathcal{Z} = Z/(\rho_0 c_0)$ is the non-dimensional surface impedance Z of the absorber, $\rho_0 c_0$ is the characteristic impedance of the ambient fluid, and $\mathrm{Re}\{\cdot\}$ and $\mathrm{Im}\{\cdot\}$ are the real and imaginary part operators, respectively. For a MAM in front of a cavity of thickness H, as illustrated in Fig. 1, the surface impedance is given by

$$Z = Z_{\mathrm{MAM}} + Z_{\mathrm{cavity}} = Z_{\mathrm{MAM}} - \mathrm{i}\rho_0 c_0 \cot(k_0 H), \tag{2}$$

where $\mathrm{i} = \sqrt{-1}$ and k_0 is the wave number. $Z_{\mathrm{MAM}} = \Delta p / v_{\mathrm{MAM}}$ is the impedance of the MAM, defined as

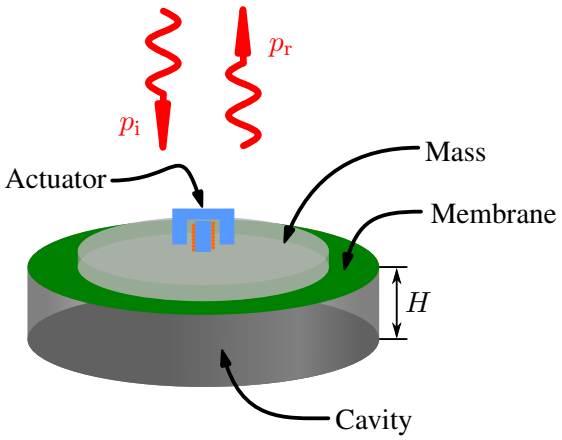

Figure 1. Illustration of the active MAM absorber unit cell.

the ratio of the pressure difference across the MAM Δp and the resulting surface-averaged MAM velocity v_{MAM}. Z_{MAM} is related to the frequency-dependent effective surface mass density of the MAM m''_{MAM} via $Z_{\mathrm{MAM}} = \mathrm{i}\omega m''_{\mathrm{MAM}}$, with the angular frequency $\omega = 2\pi f$. In the present work, it is assumed that, within the frequency range of interest, the thickness of the cavity is much smaller than the wavelength. Therefore, Eqn. (2) can be approximated by a lumped element formulation as follows:

$$Z \approx Z_{\mathrm{MAM}} + \frac{\rho_0 c_0^2}{sH}, \tag{3}$$

with $s = \mathrm{i}\omega$.

In the case of an active MAM, v_{MAM} will be a superposition of the structural response of the MAM due to the acoustic pressure field (primary path) and the force applied from the actuator (secondary path):

$$\begin{aligned} v_{\mathrm{MAM}} &= v^{(\mathrm{p})}_{\mathrm{MAM}} + v^{(\mathrm{s})}_{\mathrm{MAM}} \\ &= \frac{\Delta p}{Z^{(\mathrm{p})}_{\mathrm{MAM}}} + H_U U, \end{aligned} \tag{4}$$

where $Z^{(\mathrm{p})}_{\mathrm{MAM}}$ is the impedance of the passive MAM, $H_U = (v_{\mathrm{MAM}}/U)_{\Delta p=0}$, and U is the voltage applied at the electrical terminals of the actuator. Thus, Eqn. (3) can be reformulated for an active MAM as

$$Z \approx \frac{1}{\frac{1}{Z^{(\mathrm{p})}_{\mathrm{MAM}}} + H_U \frac{U}{\Delta p}} + \frac{\rho_0 c_0^2}{sH}. \tag{5}$$

2.2 Active MAM Model

The structural response of the active MAM to a pressure difference Δp and a point force F applied by the actuator is modelled using a state-space representation:

$$s\mathbf{x}_{\mathrm{MAM}} = \mathbf{A}\mathbf{x}_{\mathrm{MAM}} + \mathbf{B}\begin{pmatrix}\Delta p\\ F\end{pmatrix}$$
$$\begin{pmatrix}v_{\mathrm{MAM}}\\ v_F\end{pmatrix} = \mathbf{C}\mathbf{x}_{\mathrm{MAM}}. \tag{6}$$

The system matrices $\mathbf{A}$, $\mathbf{B}$, and $\mathbf{C}$ were obtained from a finite element model of the MAM [7]. Apart from the surface-averaged structural velocity of the MAM, the state-space model also outputs the structural velocity at the exciter location v_F, which will be used to couple the MAM model with the actuator model.

The actuator is modelled as a single degree-of-freedom system, as described in Ref. [9], with the actuator force F given by

$$F = Z_{\mathrm{b}} v_F + H_{\mathrm{bl}} U. \tag{7}$$

In Eqn. (7), Z_{b} is the passive base impedance of the actuator and H_{bl} is the blocked force response, which both depend on the Thiele-Small parameters of the actuator. The expressions for Z_{b} and H_{bl} were taken from Ref. [9]. Eqn. (7) was coupled with the state-space representation of the MAM in Eqn. (6), taking into account the feedback through v_F, to complete the analytical model of the active MAM.

3. RE-CONFIGURABLE MAM ABSORBER

3.1 Active MAM

The subsequent studies of different active MAM absorber configurations will be based on the same active MAM that was used in Ref. [7]. This MAM consists of a circular membrane (diameter $D = 84\,\mathrm{mm}$, to fit inside the impedance tube used in the experimental studies) made of a thin, pre-stressed polyethylene terephthalate (PET) film. A cylindrical acrylic glass mass was added to the center of the membrane, thus forming a MAM unit cell with a fundamental resonance frequency at $f_1 = 125\,\mathrm{Hz}$ and an anti-resonance frequency at 677 Hz. For the actuation of the MAM, a small Tectonic type TEAX09C005-8 electrodynamic actuator was attached to this mass. The mechanical resonance frequency of the actuator is $f_{\mathrm{ms}} = 180\,\mathrm{Hz}$. Further details and parameters of the MAM and the actuator, which were used to model the active MAM in the present contribution, can be found in Ref. [7].

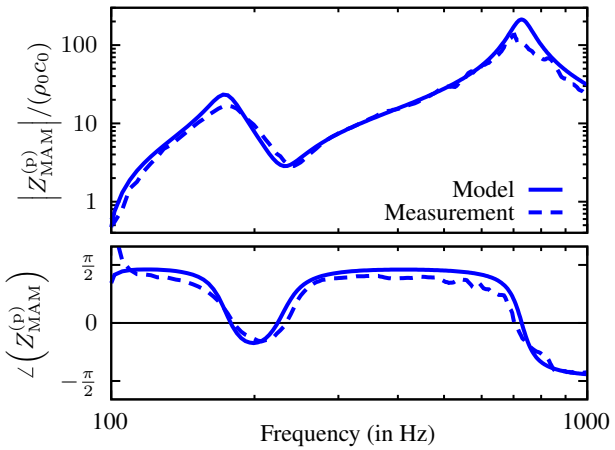

Figure 2. Comparison of the passive impedance $Z^{(\mathrm{p})}_{\mathrm{MAM}}$ of the active MAM from the analytical model with impedance tube measurements from Ref. [7].

To assess the validity of the analytical model from Section 2, the predicted passive MAM impedance $Z^{(\mathrm{p})}_{\mathrm{MAM}}$ and the plant response H_U are compared to impedance measurement data from Ref. [7]. The magnitude and phase of $Z^{(\mathrm{p})}_{\mathrm{MAM}}$ are shown in Fig. 2 for frequencies f between 100 Hz and 1000 Hz. Overall, the agreement between the analytical model and the measurement is good. The first peak in the impedance magnitude at 180 Hz corresponds to the mechanical resonance of the actuator. The second, much higher peak at around 700 Hz is related to the anti-resonance of the MAM.

The magnitude and phase of the plant response H_U are compared in Fig. 3. Again, the agreement between the experimental data and the analytical predictions is reasonably good. The main differences occur at very low frequencies (close to 100 Hz), due to inaccuracies in the measurements, and the amplitude of the peak between 200 and 300 Hz is slightly overestimated. However, the overall good agreement between the impedance tube measurements and the analytical model gives confidence in the validity of the model to explore the sound absorption of different active MAM absorber configurations in this work.

3.2 Active MAM absorber configurations

To realize the re-configurable MAM-based absorber, the aforementioned active MAM is mounted in front of a closed air cavity, as shown in Fig. 1. The thickness of the air gap was chosen to be $H = 10\,\mathrm{mm}$, to demonstrate

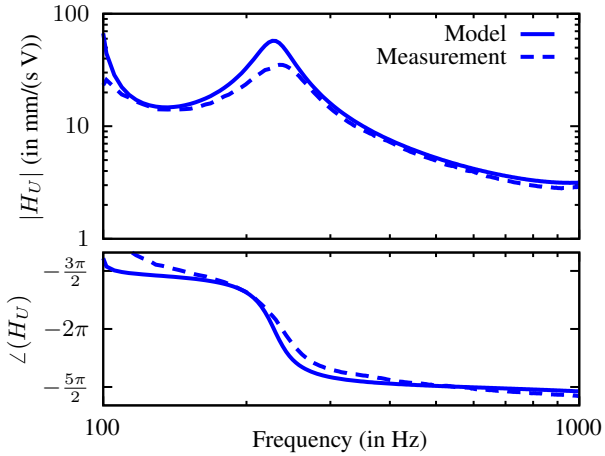

Figure 3. Comparison of the plant response of the active MAM from the analytical model with impedance tube measurements from Ref. [7].

subwavelength absorption with the MAM-based absorber.

In the following sections, three different feedback loops with the aim to achieve re-configurable sound absorption properties will be investigated using the analytical model.

3.2.1 Configuration A: Cavity pressure feedback

As shown in Fig. 4(a), in this configuration the cavity pressure p_{cav} is measured using a microphone that is placed inside the air gap. The voltage supplied to the actuator is proportional to the measured p_{cav}:

$$U = K_p p_{\mathrm{cav}}. \tag{8}$$

The gain margin of the open loop plant response (obtained using the analytical model) was used to determine the range of values of K_p, for which the feedback loop remains stable. For the given MAM absorber configuration, the stability range was determined as

$$-80.6\,\frac{\mathrm{mV}}{\mathrm{Pa}} < K_p < 13.8\,\frac{\mathrm{mV}}{\mathrm{Pa}}. \tag{9}$$

Fig. 5 shows the sound absorption coefficient α of the active MAM absorber for different values of K_p within the stability range. The black curve corresponds to the passive MAM absorber case, with $K_p = 0$. It can be seen that the passive MAM absorber exhibits a narrowband 90 % absorption peak at 390 Hz, which is typical for MAM-based subwavelength absorbers. The thickness of the absorber

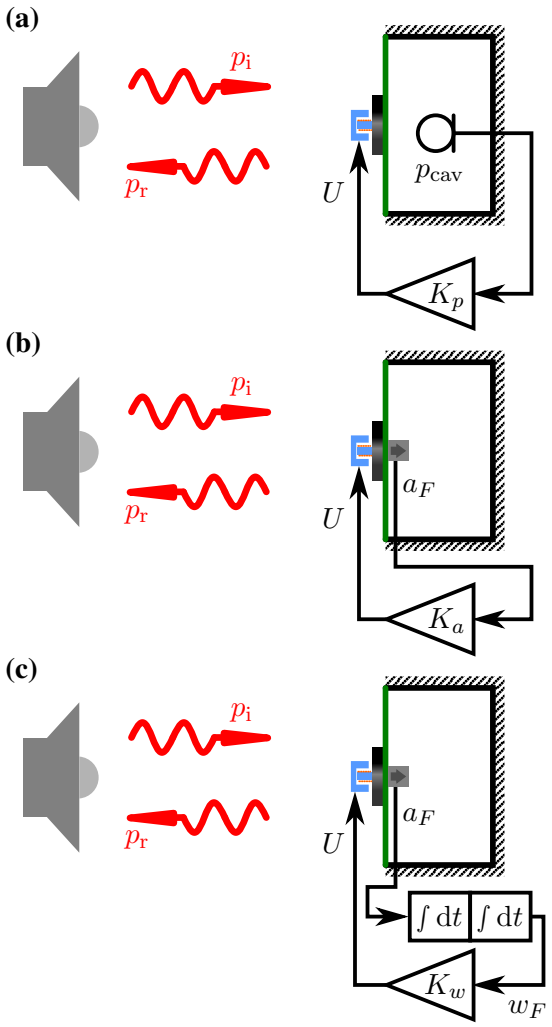

Figure 4. Illustration of the three active MAM absorber configurations investigated in this contribution. (a) Cavity pressure feedback; (b) Mass acceleration feedback; (c) Mass displacement feedback.

corresponds to just 1 % of the wavelength at the absorption peak frequency. By changing the gain value K_p, it can be seen that this active MAM configuration makes it possible to adapt the peak absorption frequency, which could be used to track and absorb a tonal frequency in the spectrum of the incident noise field. In this particular case, negative gain values lead to an increase of the absorption peak frequency, whereas positive gain values shift the absorption peak to lower frequencies. The maxi-

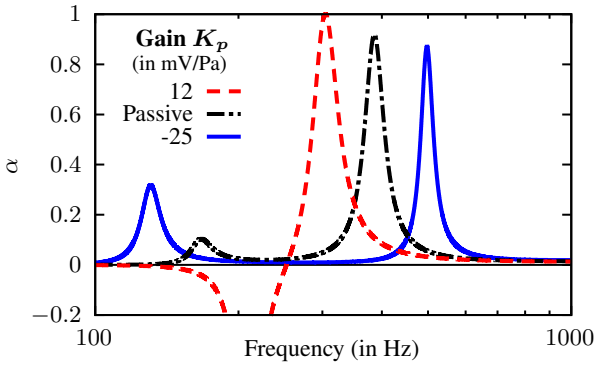

Figure 5. Sound absorption coefficient α of the active MAM absorber with cavity pressure feedback (see Fig. 4(a)) and different gain values K_p.

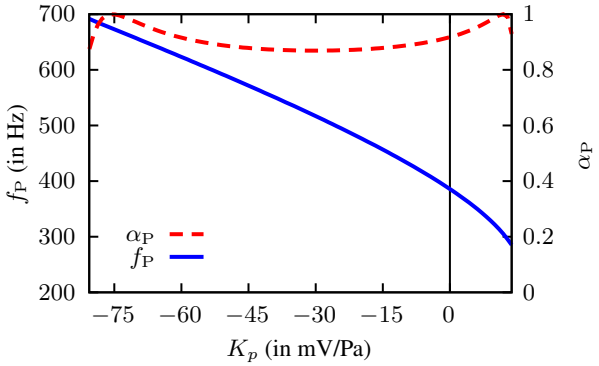

Figure 6. Relationship between the sound absorption maximum properties (frequency f_P and peak absorption α_P) and the pressure feedback gain K_p for active MAM absorber configuration A.

mum value of the absorption peak is also slightly affected by the gain, with almost perfect absorption being achieved in the case of $K_p = 12$ mV/Pa. It should also be noted that for some gain values (as in the case of $K_p = 12$ mV/Pa in Fig. 5) there can be frequency ranges with negative absorption coefficient values. This most likely happens, because in these frequency ranges the feedback loop actually amplifies the incident sound, since the sound field radiated by the MAM from the electrical excitation interferes constructively with the reflected sound field. This could be problematic for incident sound fields with significant energy content in these frequency ranges. However, if the incident sound field is dominated by tones outside these frequency ranges, the amplification caused by the active MAM absorber can be acceptable for the sake of simplicity of the active control approach.

To further illustrate the re-configurability of the sound absorption maximum of the active MAM absorber using cavity pressure feedback, Fig. 6 shows how the frequency of the absorption peak, f_P, and the maximum sound absorption coefficient α_P vary when K_p is changed (within the stability margins). It can be observed that the sound absorption peak can be moved to frequencies between 285 and 690 Hz, which spans a range of over an octave. Most notably, the absorption peak frequency can be reduced, compared to the purely passive peak frequency of 390 Hz. This implies that although the physical cavity height H remains unchanged, the active MAM absorber can be reconfigured to achieve high sound absorption values at frequencies which could only be achieved with the same passive MAM absorber using a larger cavity thickness H. As already seen in Fig. 5, the maximum absorption value α_P is only slightly affected by changing the value of K_p. For all values of K_p, α_P is well above 85 %.

3.3 Configuration B: Mass acceleration feedback

This configuration is similar to configuration A, however instead of using a microphone inside the air gap, an accelerometer is attached to the added mass of the MAM (see Fig. 4(b)). The accelerometer measures the mass acceleration a_F, which is fed back to the actuator through a proportional gain K_a:

$$U = K_a a_F. \tag{10}$$

For simplicity, it is assumed here that the mass of the accelerometer is negligibly small compared to the mass of the actuator and the added mass. This feedback configuration was determined to be stable for gain values within the range

$$-38\,\frac{\mathrm{mV\,s^2}}{\mathrm{m}} < K_a < 0.5\,\frac{\mathrm{mV\,s^2}}{\mathrm{m}}. \tag{11}$$

Fig. 7 shows the sound absorption coefficient of this active MAM absorber configuration for two different values of K_a and compares this to the sound absorption of the passive MAM absorber. The results show that since this feedback loop is mainly stable for negative values of K_a, the sound absorption peak can only be shifted towards lower frequencies. It is important to note, however, that,

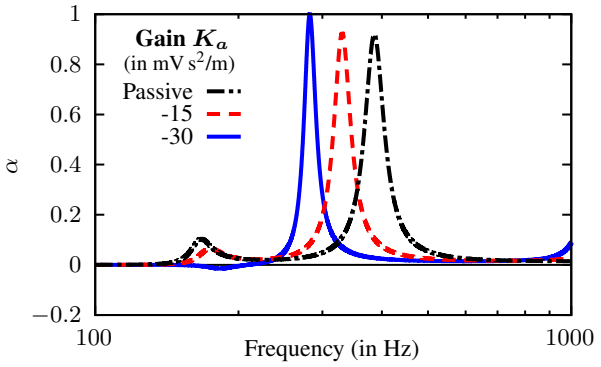

Figure 7. Sound absorption coefficient α of the active MAM absorber with mass acceleration feedback (see Fig. 4(b)) and different gain values K_a.

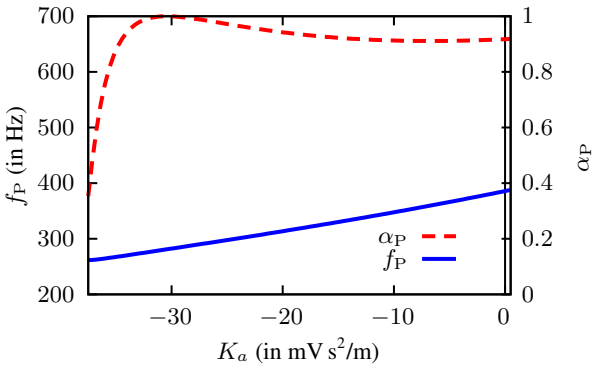

Figure 8. Relationship between the sound absorption maximum properties (frequency f_P and peak absorption α_P) and the acceleration feedback gain K_a for active MAM absorber configuration B.

when using acceleration feedback, the negative sound absorption values are not as extreme as in configuration A, even when a relatively low acceleration gain of $K_a = -30\,\mathrm{mV\,s^2/m}$ is considered. Thus, this feedback configuration may be advantageous if frequency ranges with negative absorption values should be avoided.

Fig. 8 shows how the absorption peak frequency and amplitude change when the acceleration feedback K_a is altered. It can be seen that f_P can only be reduced (compared to the passive MAM absorber) over a comparatively small frequency range between 265 Hz and 390 Hz. The minimum absorption peak frequency that can be achieved using this configuration is smaller than in the case of configuration A. However, Fig. 8 also shows that the maximum sound absorption coefficient α_P quickly drops when K_a is smaller than $-30\,\mathrm{mV\,s^2/m}$, where this active MAM absorber achieves perfect absorption. For $K_a > -30\,\mathrm{mV\,s^2/m}$, the maximum sound absorption coefficient stays consistently above 90 %.

3.4 Configuration C: Mass displacement feedback

This configuration is illustrated in Fig. 4(c). It uses the same accelerometer mounted on the added mass as in configuration B, but the acceleration signal a_F is integrated twice with respect to time in order to obtain the mass displacement w_F. The displacement signal is then fed back into the actuator after being passed through a gain K_w:

$$U = K_w w_F = K_w \frac{a_F}{s^2}. \tag{12}$$

The motivation for this configuration was that the cavity pressure p_cav, which was used in the feedback loop in configuration A, is, at low frequencies, proportional to the average MAM displacement w_MAM. Since w_MAM is difficult to measure directly and an accelerometer can easily be implemented on the added mass of an MAM, it was hoped that using w_F as a representative measure for w_MAM would yield similar results as in configuration A, where a microphone was used to measure the cavity pressure. The proposed displacement feedback loop was found to be stable for gains within the range

$$-460\,\frac{\mathrm{mV}}{\mu\mathrm{m}} < K_w < 94\,\frac{\mathrm{mV}}{\mu\mathrm{m}}. \tag{13}$$

Fig. 9 shows the absorption coefficient of this active MAM configuration at two different values of K_w. Comparing this to the results for the cavity pressure feedback in Fig. 5, it can be seen that the sound absorption of the MAM can be manipulated in almost the same way using the mass displacement feedback. The same absorption peak frequencies can be achieved (however, also the same frequency range with negative absorption for $K_w = 85\,\mathrm{mV/\mu m}$) and only the maximum absorption coefficient values are slightly different.

Fig. 10 indicates that the peak absorption frequency can be shifted between 285 Hz and 550 Hz, with f_P decreasing as K_w is increased. This range is smaller than in the case of configuration A, but with almost an octave still quite large. The peak absorption coefficient α_P remains consistently above 90 % for all stable values of K_w and

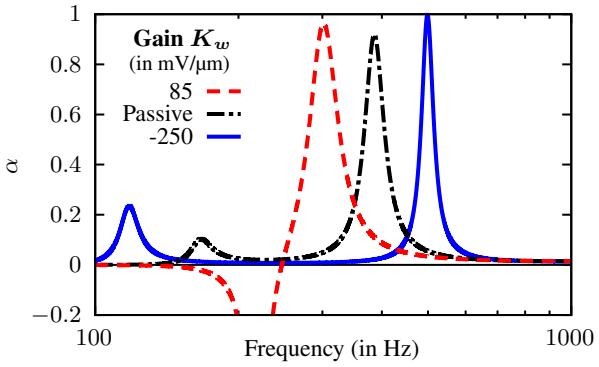

Figure 9. Sound absorption coefficient α of the active MAM absorber with mass displacement feedback (see Fig. 4(c)) and different gain values K_w.

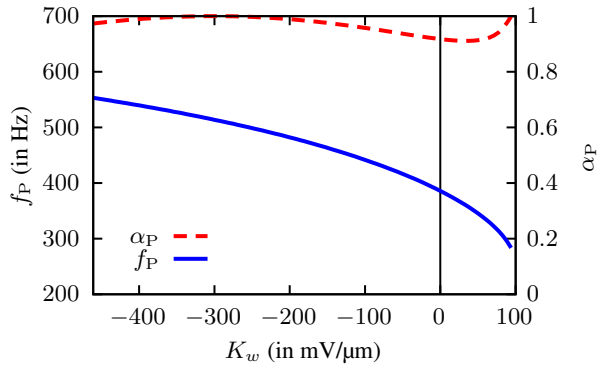

Figure 10. Relationship between the sound absorption maximum properties (frequency f_P and peak absorption α_P) and the displacement feedback gain K_w for active MAM absorber configuration C.

reaches (almost) perfect absorption for a relatively wide range of negative values of K_w.

4. CONCLUSIONS

In this work, a re-configurable subwavelength sound absorber realised using active membrane-type acoustic metamaterials (MAM), consisting of MAM with added electrodynamic actuators, was investigated. First, an analytical model of the active MAM absorber, based on the impedance of the MAM and the air cavity behind the MAM, was presented. This model was validated using impedance tube measurement data and then used to evaluate the re-configurability of the sound absorption peak of the MAM absorber with different feedback loops and a variable feedback gain. The MAM absorber design that was used to investigate the effect of the feedback on the sound absorption of the MAM had a 10 mm thick back cavity and a passive sound absorption peak frequency of 390 Hz. Three feedback configurations were compared:

- By using *cavity pressure feedback*, f_P could be re-configured within the range 285 Hz to 690 Hz with peak absorption values $\alpha_P > 85\,\%$.
- With *mass acceleration feedback*, the re-configuration range for f_P was 265 Hz to 390 Hz with $\alpha_P > 90\,\%$.
- Finally, by using *mass displacement feedback*, it was possible to tune the peak absorption frequency from 285 Hz to 550 Hz and $\alpha_P > 90\,\%$.

These results show that by using a simple feedback loop structure, the sound absorption peak of MAM can be re-configured over a wide range of frequencies and perfect absorption for thicknesses below 1 % of the wavelength can be achieved. The concepts presented here can be applied to large scale MAM absorber structures, consisting of multiple rectangular unit cells, which could open up now application of active MAM-based absorbers in noise control.

5. REFERENCES

[1] Z. Yang, J. Mei, M. Yang, N. H. Chan, and P. Sheng, "Membrane-type acoustic metamaterial with negative dynamic mass," *Physical Review Letters*, vol. 101, no. 20, p. 204301, 2008.

[2] C. J. Naify, C.-M. Chang, G. McKnight, and S. Nutt, "Transmission loss and dynamic response of membrane-type locally resonant acoustic metamaterials," *Journal of Applied Physics*, vol. 108, no. 11, p. 114905, 2010.

[3] M. Yang, Y. Li, C. Meng, C. Fu, J. Mei, Z. Yang, and P. Sheng, "Sound absorption by subwavelength membrane structures: A geometric perspective," *Comptes Rendus Mécanique*, vol. 343, no. 12, pp. 635–644, 2015.

[4] J. Mei, G. Ma, M. Yang, Z. Yang, W. Wen, and P. Sheng, "Dark acoustic metamaterials as super absorbers for low-frequency sound," *Nature Communications*, vol. 3, p. 756, 2012.

[5] T. Xing, X. Gai, J. Zhao, X. Li, Z. Cai, X. Guan, and F. Wang, "Low frequency sound absorption of adjustable membrane-type acoustic metamaterials," *Applied Acoustics*, vol. 188, p. 108586, 2022.

[6] F. Langfeldt, J. Riecken, W. Gleine, and O. von Estorff, "A membrane-type acoustic metamaterial with adjustable acoustic properties," *Journal of Sound and Vibration*, vol. 373, pp. 1–18, 2016.

[7] F. Langfeldt and J. Cheer, "Controlling the effective surface mass density of membrane-type acoustic metamaterials using dynamic actuators," *The Journal of the Acoustical Society of America*, vol. 153, no. 2, pp. 961–971, 2023.

[8] M. Möser, *Engineering Acoustics: An Introduction to Noise Control*. Berlin: Springer, 2004.

[9] J. Rohlfing, P. Gardonio, and S. J. Elliott, "Base impedance of velocity feedback control units with proof-mass electrodynamic actuators," *Journal of Sound and Vibration*, vol. 330, no. 20, pp. 4661–4675, 2011.